NANO MICRO small

Supporting Information

for *Small,* DOI: 10.1002/smll.202200311

Ultraflexible and Stretchable Intrafascicular Peripheral Nerve Recording Device with Axon-Dimension, Cuff-Less Microneedle Electrode Array

*Dongxiao Yan, Ahmad A. Jiman, Elizabeth C. Bottorff, Paras R. Patel, Dilara Meli, Elissa J. Welle, David C. Ratze, Leif A. Havton, Cynthia A. Chestek, Stephen W. P. Kemp, Tim M. Bruns, Euisik Yoon, and John P. Seymour**

Support Information

Ultra-flexible and Stretchable Intrafascicular Peripheral Nerve Recording Device with Axon-dimension, Cuff-less Microneedle Electrode Array

Dongxiao Yan[1], Ahmad A. Jiman[2,3], Elizabeth C. Bottorff[3], Paras R. Patel[3], Dilara Meli[4], Elissa J. Welle[3], David C. Ratze[1], Leif A. Havton[5,6], Cynthia A. Chestek[3], Stephen W.P. Kemp[3,7], Tim M. Bruns[3], Euisik Yoon[1,3,8], John Seymour[1,9,10]*

[1]Department of Electrical Engineering and Computer Science, University of Michigan, Ann Arbor, MI.
[2]Department of Electrical and Computer Engineering, King Abdulaziz University, Jeddah, Saudi Arabia.
[3]Department of Biomedical Engineering, University of Michigan, Ann Arbor, MI.
[4]Department of Materials Science and Engineering, Northwestern University, Evanston, IL.
[5]Departments of Neurology and Neuroscience, Icahn School of Medicine at Mount Sinai, New York, NY.
[6]James J Peters Veterans Affairs Medical Center, Bronx, NY
[7]Section of Plastic Surgery, University of Michigan, Ann Arbor, MI.
[8]Center for Nanomedicine, Institute for Basic Science (IBS) and Graduate Program of Nano Biomedical Engineering (Nano BME), Advanced Science Institute, Yonsei University, Seoul, South Korea.
[9]Department of Neurosurgery, UTHealth, Houston, TX.
[10]Department of Electrical and Computer Engineering, Rice University, Houston, TX.
***Corresponding author**

Contents

Table S1. Comparison of tensile (t) and shear (s) strengths of various tissue adhesives.

Adhesive	Strength (kPa)	Substrate	Curing Agent, Time/Dosage	Adhesive Type	Reference & Note
Rose bengal	3.41 ±1.96 (t)	Sciatic nerve, PDMS/ParC	Green light, 300 J/cm^2 @ 60W/cm^2	Dry	This Work
	7.12 ± 4.71 (t)	Sciatic nerve, PDMS/ParC (+collagen)			
	18.2 ± 13.4 (s)	Sciatic nerve, PDMS/ParC (+collagen)			
	34.6 ± 22.6 (t)	Sciatic nerve, PU			
	26.7 ± 18.1 (t)	Sciatic nerve, PU (+collagen)			
Cyanoacrylate	46.67 ± 12.13 (t)	Porcine vocal folds	Air, 5minutes	Wet	[1]
	68.79 ± 13.29 (s)	Porcine vocal folds	Air, 5 minutes		
	21 ± 60 (t)	Porcine skin	Air, 60-90 seconds		[2]
	32.6 ± 89 (s)	Porcine skin	Air, 60-90 seconds		
Fibrin glue	10.7 ± 6.42 (t)	Porcine vocal folds	Thrombin, 60 minutes	Wet	[1]
	13.86 ±5.03 (s)	Porcine vocal folds	Thrombin, 60 minutes		
	0.7 ± 0.6 (t)	Porcine skin	Thrombin, 2 hours		[2]
	2.2 ± 1.3 (s)	Porcine skin	Thrombin, 2 hours		
UVA-riboflavin [a]	13.6 ± 1.0 (s)	Cornea	370 nm, 4.5 min @ 30 mW/cm^2	Wet	[3]
Polydopamine	60.13 ±7.67 (t)	PDMS-PDA/PDMP	Incubate for 1 hour		[4]
	28.5 (s)	Adhesive hydrogel to porcine skin	None, Immediate		[5]

Note to Table S1: Medical-grade polyurethane (PU) as a device surface can offer greater adhesive strength than PDMS, but this elastomer was not available for spin-on or embossing applications.

Table S2. Fixed-effect analysis using generalized linear mixed model for each Group against Control group.

	Group	*Estimate*	*Std. error*	*z value*	*Pr* (>|z|)	
Distal & Proximal	*1w MINA*	-1.34673	0.28293	-4.76	1.94E-06	***
	1w Sham	-0.46565	0.28246	-1.649	0.0992	.
	6w MINA	-0.43562	0.29565	-1.473	0.1406	
	6w Sham	-0.02143	0.31577	-0.068	0.9459	
Distal	*1w MINA*	-1.793436	0.313318	-5.724	1.04e-08	***
	1w Sham	-1.011510	0.298228	-3.392	0.000695	***
	6w MINA	-0.534037	0.311181	-1.716	0.086133	.
	6w Sham	-0.001098	0.332431	-0.003	0.997364	
Proximal	*1w MINA*	-1.33071	0.41129	-3.235	0.00121	**
	1w Sham	-0.27218	0.41061	-0.663	0.50741	
	6w MINA	-0.386416	0.42929	-0.900	0.3680	
	6w Sham	-0.08697	0.45906	-0.189	0.84973	
	p-value code	<0.001 '***'	0.001-0.01 '**'	0.01-0.05 '*'	0.05-1 '.'	>1 ''

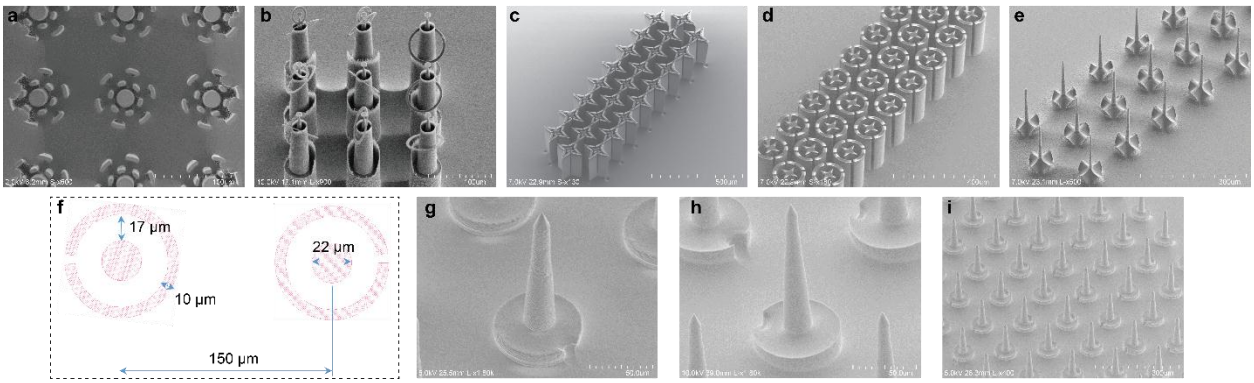

Figure S1. A variety of silicon microneedle shaping by deep reactive ion etching and reactive ion etching. **a).** A double pilar arrangement, **b)** double sacrificial shield, **c)** a cross-shaped needle and sacrificial shield, **d)** a cross-shaped needle and circular sacrificial, and **e)** and the narrowest needle attempted, which suffered from fracture during insertion. **f).** Final mask pattern for a 150-µm pitch microneedle. **g).** The post-etch roughness resulted from the scalloping of DRIE and the isotropic plasma etch. **h-i).** After thermal SiO_2 was grown on the surface and a brief hydrofluoric acid etch, a smooth surface was formed and was highly scalable.

Note on Fig. S1: Our initial attempts at making sacrificial pillars, Fig. S1(a) was inspired by Hanein et al.[6]. This lacked the smoothness and taper control desired for the needle sidewalls, so we settled on sacrificial cylinders with at least one slit for plasma reactant and product exchange. These slits left an artifact structure in the needle base but greatly improved the uniformity of each needle taper. As first described in Yan et al.[7], the timing for each anisotropic and isotropic stage was approximated with modeling of the etch, but ultimately required empirical evaluation to finalize the etch recipe specific to a given tool. Some of the advanced geometries, such as (c) and (d) were not fully optimized for use here but may provide a way to improve the strength of a needle while reducing the cross-sectional area.

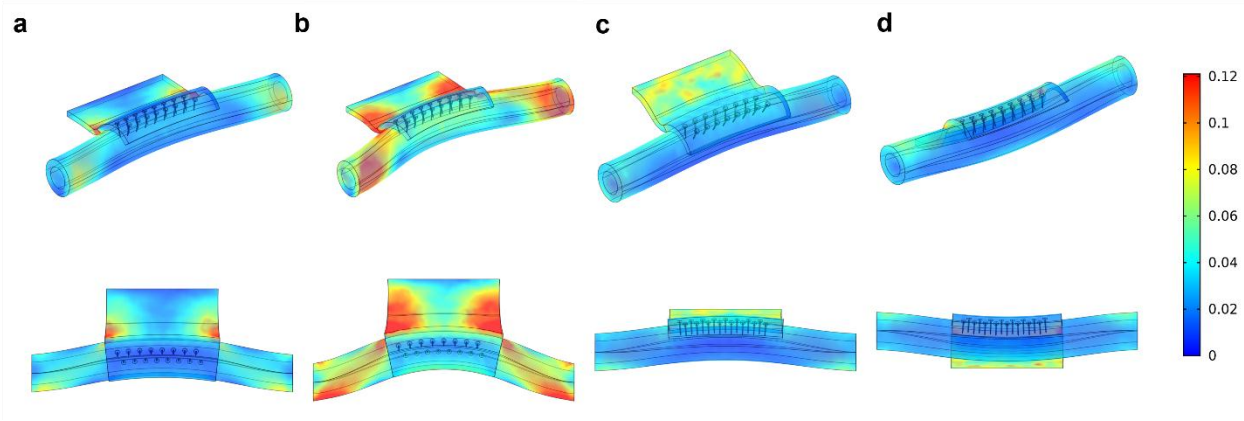

Figure S2. Distribution of the first principal strain across a single-fascicle nerve under tethered displacement after implantation with a MINA device. Strain on the modeled tissue and device is induced by the movement of the tethered end by applying a displacement of **a)** 250 μm and **b).** 500 μm lateral; and **c)** +500 μm and **d)** -500 μm vertical directions. The far ends of the nerve are fixed 1 mm from the edge of MINA. Nerve diameter = 500 μm.

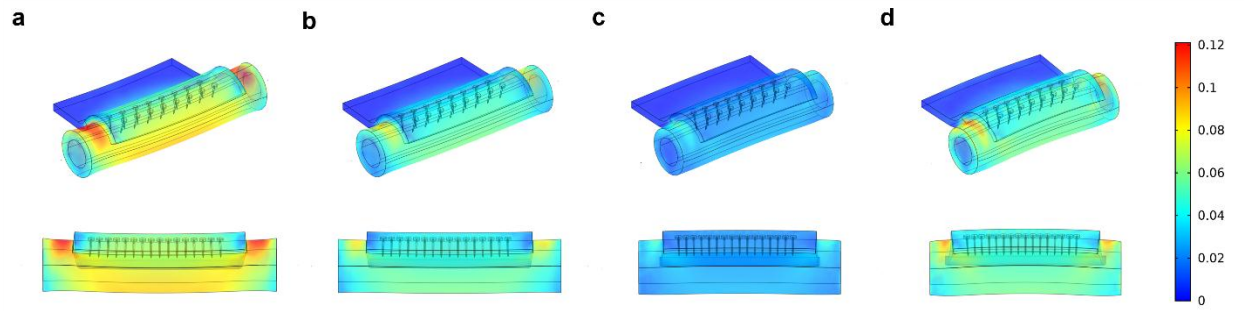

Figure S3. Distribution of the first principal strain across a single-fascicle nerve under axial tension or compression after implantation with a MINA device. The axial strain is applied to the ends of a 2-mm long nerve section as **a).** 10% tensile; **b).** 5% tensile; **c).** 5% compressive; and **d).** 10% compressive. Nerve diameter = 500 μm.

Note on Fig. S2, S3: This COMSOL finite element model assumed that there was attachment between MINA silicone surface and the epineurium, such as would be created with the adhesive procedure used in this study. The Young's modulus of the epineurium, endoneurium, and device substrate was set to be 1 MPa, 10 kPa 1.32 MPa. Elastic properties of the nerve were assumed, making this only a rough estimation of the strain profile given a viscoelastic should be more precise if these parameters were known. The diameter of the nerve model is 500 μm. The thickness of the epineurium layer is 100 μm. Others have demonstrated that the tensile modulus of most peripheral nerves ranges from 10 kPa to 2 MPa [8–10]. The variance of this value comes from a difference of the sizes and types of the nerves tested. The epineurium layer has a higher elastic modulus compared with the composite nerve. The substrate material (PDMS) used in this paper has a similar Young's modulus. Figure S3 shows the modeling of a MINA-implanted nerve under compressive strain. The 5% compressive simulation estimated the strain distribution over the nerve being released from the holder and relaxed to its initial size after implantation.

An important implication of these models suggests that the most vulnerable portion of the nerve will be the adjacent nerve portions just proximal and distal to an attached device. It also suggests that the microneedles do not induce local damage. Note that these apply to the condition of uniform adhesion to the epineurium. More complex models should also study the gradient condition when the edges of the attached device begin to delaminate. Finally, it is worth noting that the device will eventually scar in due to collagenous tissue encapsulation as evidenced in our micro-CT images and numerous other studies, which will reduce localized damage. More research is needed but these models support the need for strong adhesion for at least some period post implantation.

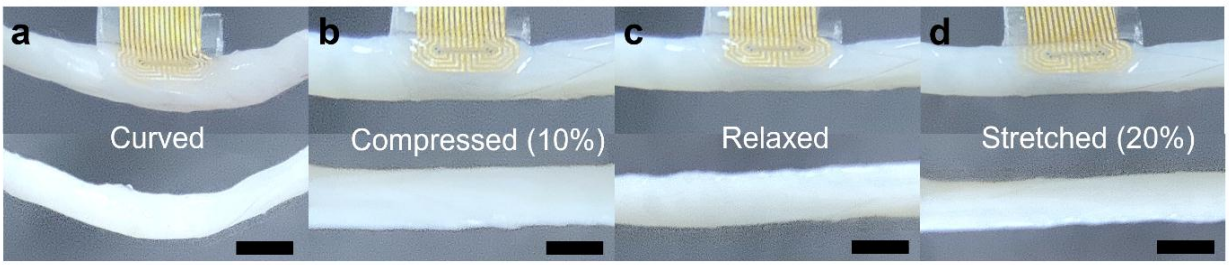

Figure S4. Demonstration of a sciatic nerve under compression and tension with a MINA device implanted. Images of a). curved, b). compressed, c). relaxed, and d). stretched up to 20%. Samples in top row are implanted with MINA and the bottom row is for comparison with a nerve without MINA implantation. Scale = 500 μm.

Note on Fig. S4: The conditions (b) and (d) support the results in S3c and S3a, respectively. At condition (c), the nerve sample was resting at its natural length.

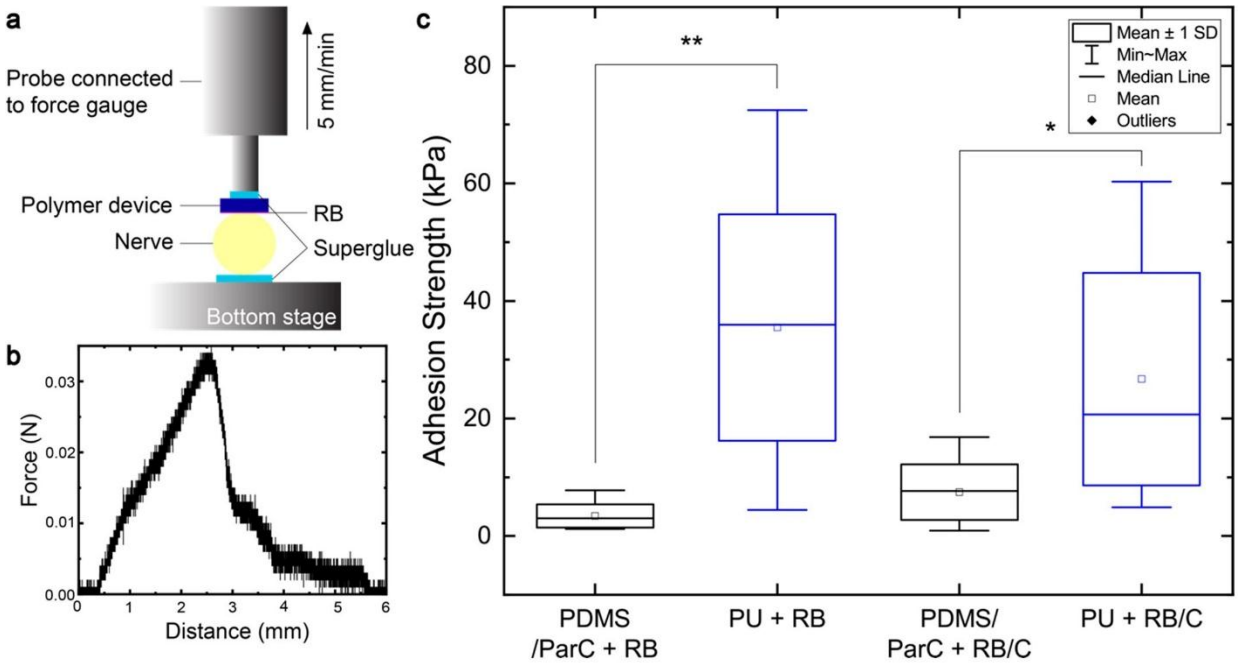

Figure S5. Tensile strength measurements of MINA after rose bengal activation. **a).** Tensile adhesion strength testing setup. **b).** Representative pulling force vs. traveling distance during a single tensile adhesion strength test. **c).** Adhesion strength of devices with different surface and coating to sciatic nerves attached via photochemical tissue bonding (N=10).

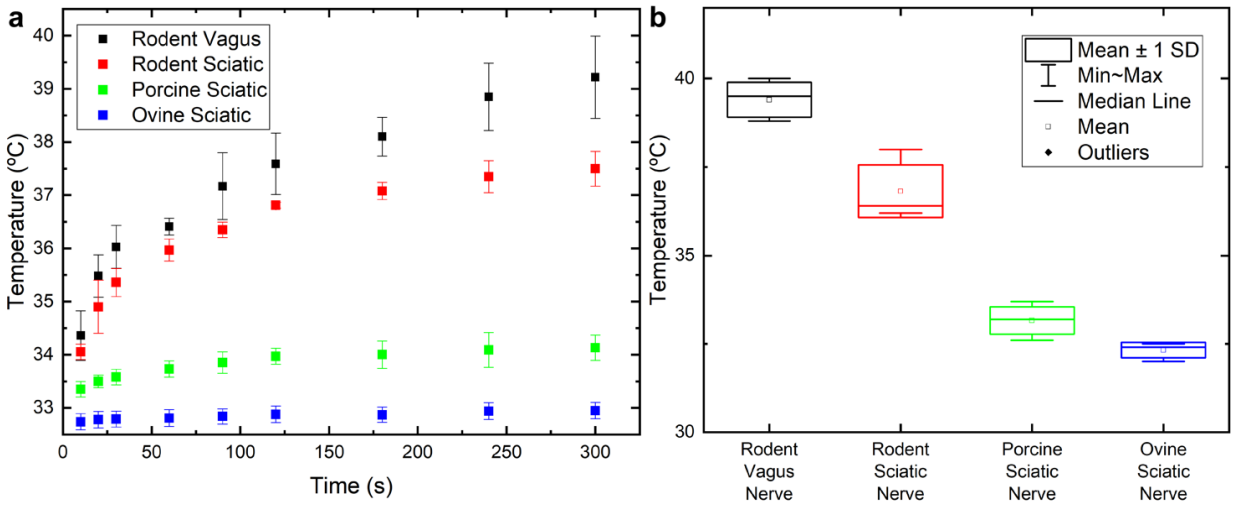

Figure S6. *In vitro* temperature measurements during and after rose bengal light activation. **a).** *In vitro* temperature increase of rodent vagus and rodent, porcine, and ovine sciatic nerves upon irradiation. **b).** Maximum temperature increase of rodent vagus and rodent, porcine, and ovine sciatic nerves after 300 seconds of irradiation at 1 W/cm^2 (N=5).

Note on Fig. S6: The nerve samples used here were extracted and kept refrigerated in saline for less than 24 hours. Before measurement, the saline was heated to 37 ℃. The samples were loaded onto the trench of the lens-attached nerve holder (Figure S7c). Irradiation was applied through the diffusion lens. Temperature was measured with an infrared camera (Seek Thermal®)

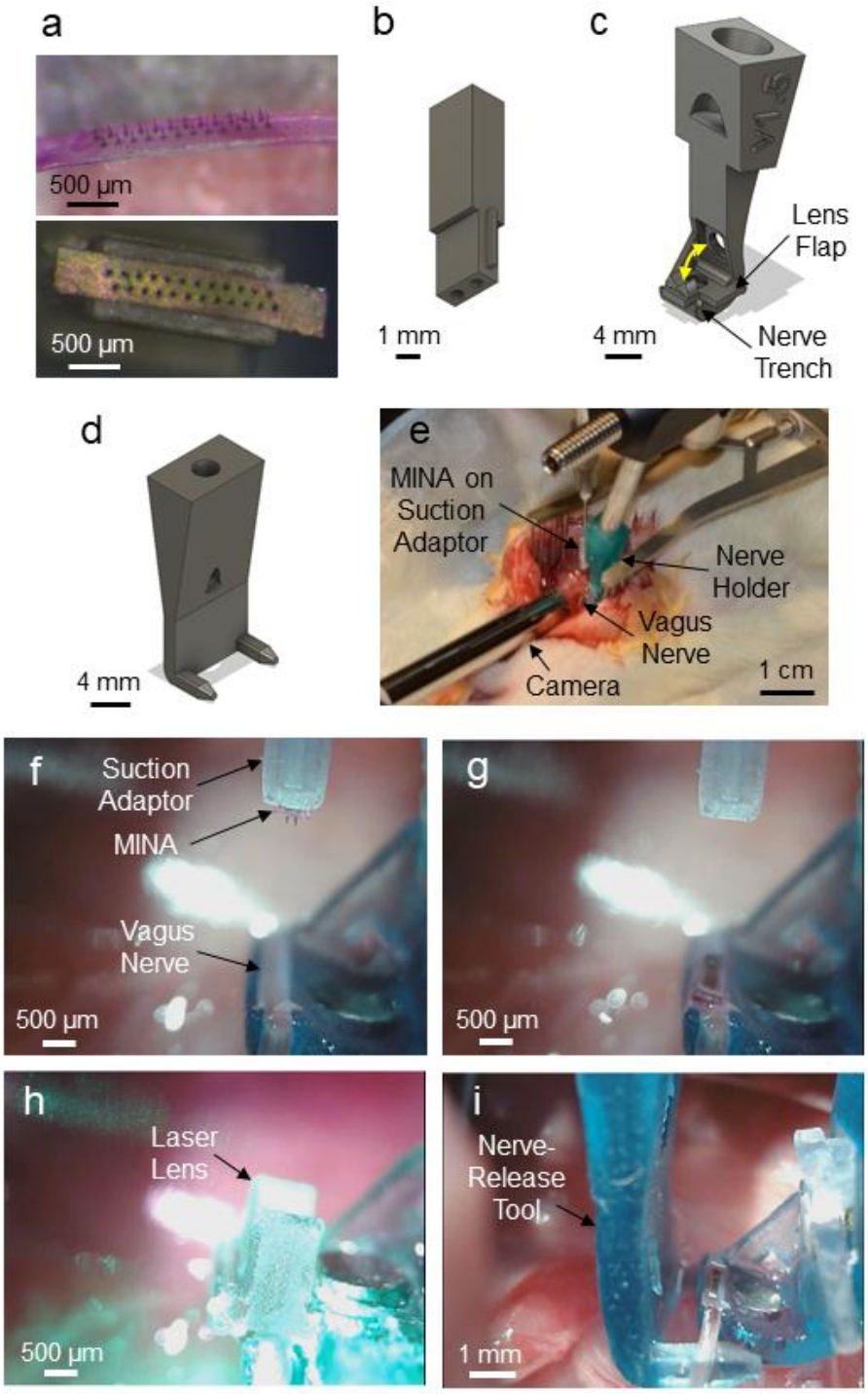

Figure S7. Implantation of rose bengal coated MINA. **a).** Rose bengal coated MINA with 2x12 needle configuration (top). MINA centered on vacuum suction adapter (bottom). **b).** Design of vacuum suction adapter. **c).** Nerve-holder design. Yellow arrows show movement path of lens flap. **d).** Design of a separate nerve-release tool. **e).** Surgical setup for implantation in vagus nerve. **f).** View from pen camera for aligning MINA. **g).** MINA inserted in vagus nerve. **h).** Placement of lens flap and activation of rose bengal coating with laser. **i).** Release of MINA-implanted vagus nerve from the nerve holder with the nerve-release tool.

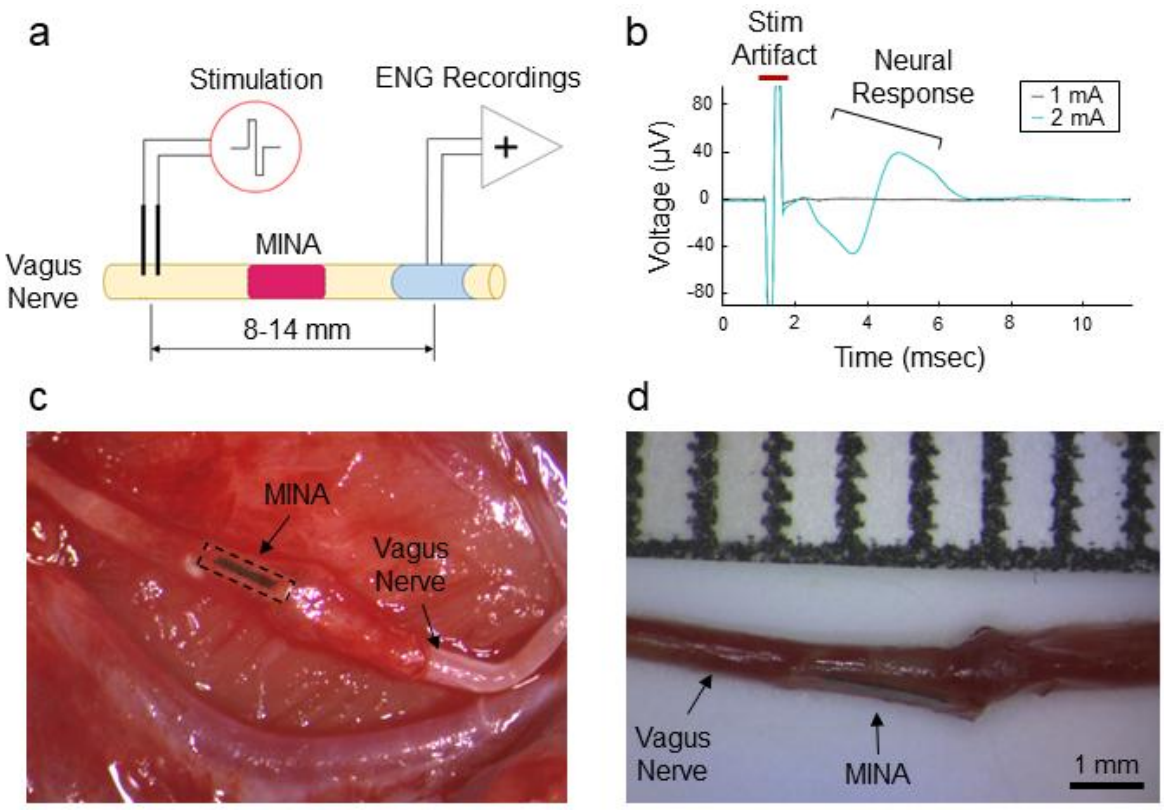

Figure S8. Electrophysiology testing and nerve extraction at a terminal procedure. **a).** Setup diagram for electrophysiology testing. **b).** Example stimulation-evoked compound action potential responses in one rat. **c).** Isolation (top-down view) and **d).** extraction (side view) of MINA-implanted vagus nerve for a 1-week rat.

REFERENCE

[1] L. X. Chen, M. Coulombe, F. Barthelat, A. Rammal, L. Mongeau, K. Kost, *Laryngoscope* **2019**, DOI 10.1002/lary.27769.

[2] S. Kull, I. Martinelli, E. Briganti, P. Losi, D. Spiller, S. Tonlorenzi, G. Soldani, *J. Surg. Res.* **2009**, *157*, e15.

[3] T. G. Seiler, M. Engler, E. Beck, R. Birngruber, I. E. Kochevar, *Investig. Ophthalmol. Vis. Sci.* **2017**, DOI 10.1167/iovs.17-22426.

[4] M. Kim, K. H. Song, J. Doh, *Colloids Surfaces B Biointerfaces* **2013**, DOI 10.1016/j.colsurfb.2013.07.021.

[5] L. Han, X. Lu, K. Liu, K. Wang, L. Fang, L. T. Weng, H. Zhang, Y. Tang, F. Ren, C. Zhao, G. Sun, R. Liang, Z. Li, *ACS Nano* **2017**, *11*, 2561.

[6] Y. Hanein, C. G. J. Schabmueller, G. Holman, P. L cke, D. D. Denton, K. F. B hringer, *J. Micromechanics Microengineering* **2003**, *13*, S91.

[7] D. Yan, A. Jiman, D. Ratze, S. Huang, S. Parizi, E. Welle, Z. Ouyang, P. Patel, M. J. Kushner, C. Chestek, T. M. Bruns, E. Yoon, J. Seymour, in *Int. IEEE/EMBS Conf. Neural Eng. NER*, **2019**.

[8] M. K. Kwan, E. J. Wall, J. Massie, S. R. Garfin, *https://doi.org/10.3109/17453679209154780* **2009**, *63*, 267.

[9] M. J. Alexander, J. M. Barkmeier-Kraemer, J. P. V. Geest, *Ann. Biomed. Eng.* **2010**, *38*, 2553.

[10] C. T. Liu, C. E. Benda, F. H. Lewey, *Arch. Neurol. Psychiatry* **1948**, *59*, 322.